RevMexAA (Serie de Conferencias), **36**, 37–44 (2009)

STUDYING ISM MAGNETIC FIELDS AND TURBULENT REGIMES FROM POLARIMETRIC MAPS

D. Falceta-Gonçalves,[1,2] A. Lazarian,[2] and G. Kowal[3]

RESUMEN

Mapas polarimétricos han sido usados para caracterizar el campo magnético en nubes moleculares. Sin embargo, es difícil determinar las propiedades tridimensionales de mapas de proyección de dichas regiones. Por esta razón, simulaciones numéricas pueden ser usadas como pruebas de las mediciones polarimétricas, y eventualmente revelar más acerca de la relación entre la turbulencia y las líneas de campo magnético. En este trabajo realizamos una serie de simulaciones MHD de nubes moleculares turbulentas y creamos mapas sintéticos de emisión polarizada de polvo, en las cuales variamos la dirección del observador. Determinamos la correlación de la intensidad de la emisión y el grado de polarización para los modelos. Pudimos reproducir el decaimiento del grado de polarización en zonas más densas sin suposición alguna de las propiedades de la componente de polvo. La anticorrelación viene la simple cancelación de los vectores de polarización a lo largo de la visual. El efecto es amplificado dentro de zonas de alta densidad ya que la configuración del campo magnético se torna más compleja. Estudiamos la función de distribución de probabilidad, el espectro de potencias, y funciones de estructura de los ángulos de polarización. Estos análisis estadísticos revelan gandres diferencias dependiendo del régimen turbulento (es decir sub ó súper-sónico, sub ó super-Alfvénico). Entonces, estos métodos pueden ser utilizados en observaciones polarimétricas para caracterizar la dinámica de las nubes moleculares. Presentamos también un método Chandrassekhar-Fermi modificado para obtener la magnitud del campo magnético local. La formulación sugerida no muestra limitaciones respecto al régimen turbulento u orientación.

ABSTRACT

Polarimetric maps have been used for the characterization of the magnetic field in molecular clouds. However, it is difficult to determine the 3-dimensional properties of these regions from the projected maps. For that reason, numerical simulations can be used as benchmarks for polarimetric measurements, and eventually reveal more about the interplay of turbulence and the magnetic field lines. In this work we make a number of MHD numerical simulations of turbulent molecular clouds and created their synthetic dust emission polarization maps, varying the direction of the observer. We determined the correlation of intensity emitted and polarization degree for the simulated models. We were able to reproduce the decay of the polarization degree at denser regions without any assumption regarding the properties of the dusty component. The anti-correlation arises from the simple cancellation of the polarization vectors along the line of sight. This effect is amplified within denser regions as the magnetic field configuration becomes more complex. We studied the probability distribution function, the power spectrum, and the structure function of the polarization angles. This statistical analysis revealed strong differences depending on the turbulent regime (i.e. sub/supersonic and sub/super-Alfvenic). Therefore, these methods can be used on polarimetric observations to characterize the dynamics of molecular clouds. We also presented a modified Chandrashekhar-Fermi method to obtain the intensity of the local magnetic field. The proposed formulation showed no limitations regarding orientation or turbulent regime.

Key Words: ISM: magnetic fields — methods: numerical — methods: statistical — techniques: polarimetric

1. INTRODUCTION

Giant molecular clouds in the interstellar medium (ISM) are believed to be threaded by large scale magnetic fields (Schleuning 1998; Crutcher et al. 1999). However, it is still not completely clear what is the role of the magnetic field in the dynamics of the ISM and what is its effect on the star formation process. Also, the ratio of the magnetic and turbulent energy in these environments is a subject of controversy (Padoan & Norlund 2002; Girart, Rao, & Marrone 2006). Polarimetric maps have been extensively used for the determination of the magnetic

[1]Núcleo de Astrofísica Teórica, Universidade Cruzeiro do Sul, Rua Galvão Bueno 868, CEP 01506-000, São Paulo, Brazil (diego.goncalves@unicsul.br).

[2]Astronomy Department, University of Wisconsin, Madison, 475 N. Charter St., WI 53711, USA.

[3]Astronomical Observatory, Jagiellonian University, ul. Orla 171, 30-244 Kraków, Poland.

fields in several astrophysical environments. This technique represents the best tool to characterize the vector components of the magnetic field parallel to plane of the sky. For galaxies and the intracluster medium this technique can be used for polarization of synchrotron emission (Hildebrand et al. 2000).

For a given polarization map of an observed region, the mean polarization angle indicates the orientation of the large scale magnetic field. On the other hand the polarization dispersion gives clues on the value of the turbulent energy. This, as a consequence, can be used to determine the magnetic field component in the plane of sky. Chandrasekhar & Fermi (1953) introduced a method (hereafter CF method) for estimating the ISM magnetic fields based on the dispersions of the polarization angle and gas velocity. Simply, it is assumed that the magnetic field perturbations are Alfvenic and that the rms velocity is isotropic.

A promising approach to test this method is to create two-dimensional (plane of sky) synthetic maps from numerically simulated cubes. Ostriker, Stone, & Gammie (2001) performed 3D-MHD simulations, with 256^3 resolution, in order to obtain polarization maps and study the validity of the CF method on the estimation of the magnetic field component along the plane of sky. They showed that the CF method gives reasonable results for highly magnetized media, in which the dispersion of the polarization angle is $< 25°$. However, they did not present any other statistical analysis or predictions that could be useful to determine the ISM magnetic field from observations. Polarization maps from numerical simulations can also be used in the study of the correlation between the polarization degree and the total emission intensity (or dust column density). Observationally, the polarization degree in dense molecular clouds decreases with the total intensity as $P \propto I^{-\alpha}$, with $\alpha = 0.5 - 1.2$ (Gonçalves, Galli, & Walmsley 2005). Padoan et al. (2001) studied the role of turbulent cells in the P *vs* I relation using supersonic and super-Alfvenic self-gravitating MHD simulations. They found a decrease of the polarization degree with total dust emission within gravitational cores, in agreement with observations, if grains are assumed to be unaligned for $A_V > 3$. When the alignment was assumed to be independent on A_V, the anti-correlation was not observed. Recently, Pelkonen, Juvela, & Padoan (2007) extended this work and refined the calculation of polarization degree introducing the radiative transfer properly. In that work, the decrease in the alignment efficiency arises without any *ad hoc* assumption. The alignment efficiency decreases as the radiative torques become less important in the denser regions. However, it is still not clear the role of the magnetic field topology and the presence of multiple cores intercepted by the line of sight on the decrease of polarization degree.

In this work we attempt to extend the previously cited studies improving and applying the CF method to different situations. For that, we used both sub and super-Alfvenic models, to study the role of the magnetic field topology in the observed polarization maps.

2. NUMERICAL SIMULATIONS

The simulations were performed solving the set of ideal MHD equations, in conservative form, as follows:

$$\frac{\partial \rho}{\partial t} + \nabla \cdot (\rho \mathbf{v}) = 0\,, \quad (1)$$

$$\frac{\partial \rho \mathbf{v}}{\partial t} + \nabla \cdot \left[\rho \mathbf{v}\mathbf{v} + \left(p + \frac{B^2}{8\pi}\right)\mathbf{I} - \frac{1}{4\pi}\mathbf{B}\mathbf{B}\right] = \rho \mathbf{f}\,, \quad (2)$$

$$\frac{\partial \mathbf{B}}{\partial t} - \nabla \times (\mathbf{v} \times \mathbf{B}) = 0\,, \quad (3)$$

with $\nabla \cdot \mathbf{B} = 0$, where ρ, $\mathbf{v}$ and p are the plasma density, velocity and pressure, respectively, $\mathbf{B}$ is the magnetic field and $\mathbf{f}$ represents the external acceleration source, responsible for the turbulence injection. For molecular clouds, we may assume that the ratio of dynamical to radiative timescales is very large. Under this assumption, the set of equations is closed with an isothermal equation of state $p = c_s^2 \rho$, where c_s is the speed of sound. The equations are solved using a second-order-accurate and non-oscillatory scheme, with periodic boundaries, as described in Kowal, Lazarian, & Beresniak (2007).

Initially, we set the intensity of the x-directed magnetic field $\mathbf{B_{ext}}$ and the gas thermal pressure p. This allows us to obtain sub-Alfvenic or super-Alfvenic, and subsonic or supersonic models.

The turbulent energy is injected using a random solenoidal function for $\mathbf{f}$ in Fourier space. This, in order to minimize the influence of the forcing in the formation of density structures. We inject energy at scales $k \propto L/l < 4$, where L is the box size and l is the eddy size of the injection scale. The rms velocity δV is kept close to unity, therefore $\mathbf{v}$ and the Alfvén speed $v_A = B/\sqrt{4\pi\rho}$ will be measured in terms of the rms δV. Also, the time t is measured in terms of the dynamical timescale of the largest turbulent eddy ($\sim L/\delta V$).

We performed four computationally extensive 3D MHD simulations, using high resolution (512^3), for

TABLE 1

DESCRIPTION OF THE SIMULATIONS

Model	P	$B_{\rm ext}$	Description
1	1.00	1.00	subsonic & sub-Alfvenic
2	0.10	1.00	supersonic & sub-Alfvenic
3	0.01	1.00	supersonic & sub-Alfvenic
4	0.01	0.10	supersonic & super-Alfvenic

different initial conditions, as shown in Table 1. We simulated the clouds up to $t_{\rm max} \sim 5$, i.e. 5 times longer than the dynamical timescale, to ensure a full development of the turbulent cascade. We obtained one subsonic and three supersonic models. One of the supersonic models is also super-Alfvenic. Each data cube contains information about parameterized density, velocity and magnetic field. As noted from equation (1) and (2), the simulations are non self-gravitating and, for this reason, the results are scale-independent.

Regarding the gas distribution in each model we found an increasing contrast as we go to higher sonic Mach number, independently on the Alfvenic Mach number. Subsonic turbulence show a gaussian distribution of densities, while the increased number and strength of shocks in supersonic cases create smaller and denser structures. In these cases, the density contrast may be increased by a factor of 100–10000 compared to the subsonic case. The magnetic field topology, on the other hand, depends on the Alfvenic Mach number. Sub-Alfvenic models show a strong uniformity of the field lines, while the super-Alfvenic case shows a very complex structure. Both effects, the density contrast and the magnetic field topology, may play a role on the polarimetric maps, as shown further in the paper.

3. RESULTS

3.1. *Polarization Maps*

To create the polarization maps we assumed the dust polarization to be completely efficient and that the radiation is originated exclusively by thermal emission from perfectly aligned grains. Under these assumptions, the local angle of alignment (ψ) is determined by the local magnetic field projected into the plane of sky, and the linear polarization Stokes parameters Q and U are given by:

$$\begin{aligned} q &= \rho \cos 2\psi \sin^2 i, \\ u &= \rho \sin 2\psi \sin^2 i, \end{aligned} \qquad (4)$$

where ρ is the local density and i is the inclination of the local magnetic field and the line of sight. We then obtain the integrated Q and U, as well as the column density, along the LOS. Notice that, for the given equations the total intensity (Stokes I) is assumed to be simply proportional to the column density. The polarization degree is calculated from $P = \sqrt{Q^2 + U^2}/I$ and the polarization angle $\phi = a\ \tan(U/Q)$.

In Figures 1 and 2 (see Falceta-Gonçalves, Lazarian, & Kowal 2008, hereafter FLK08), we show the obtained maps of column density and the polarization vectors for Models 3 and 4, respectively, for a line of sight perpendicular to the original magnetic field orientation. In Figure 1, the polarization vectors are mostly uniform, and parallel to the external magnetic field. Here, fluctuations on the polarization angle are seen within the condensations, where the kinetic pressure overcomes the magnetic pressure. In Figure 2, we show the column density and polarization maps of the super-Alfvenic case (Model 4). Here, the kinetic energy is larger than the magnetic pressure almost everywhere. As a consequence the gas easily tangles the magnetic field lines. The angular dispersion is larger and the polarization degree is smaller when compared to the sub-Alfvenic case. For the super-Alfvenic case, the orientation of the magnetic field regarding the LOS is irrelevant to the polarization maps. The strongly magnetized cases (Models 1, 2 and 3) present very similar polarization maps. Also, we must note that for LOS parallel to the original magnetic field, the polarization maps seem similar to the super-Alfvenic case.

Regarding the polarization degree, observations have shown that a decorrelation between the polarization degree and the column densities is detected for several objects (Matthews & Wilson 2002; Lai, Girart, & Crutcher 2003; Wolf, Launhardt, & Henning 2003). Typically, the polarization degree follows the relation $P \propto I^{-\gamma}$, where $\gamma \sim 0.5 - 1.2$ (Gonçalves, Galli, & Walmsley 2005) and I is the total intensity. Usually, it is assumed that the grain alignment efficiency may be the general cause of this effect. However, as noticeable from Figures 1 and 2, the polarization degree is smaller within high column density regions for all models. Note that we assumed perfect grain alignment, independent on the local density. Therefore, the decorrelation in our simulations must have a different cause. Another possibility could be the effect of the averaging along the LOS. Denser regions present a less uniform magnetic field. The annihilation of polarization vectors perpendicular to each other could cause the decrease in the polarization degree.

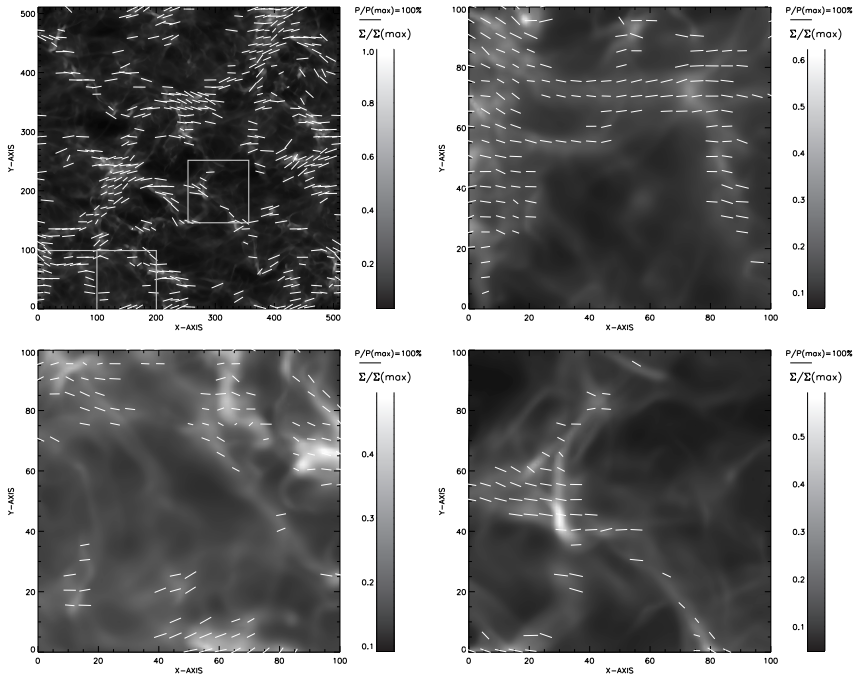

Fig. 1. Polarization of emission and column density maps for Model 3 ($M_{\rm S} \sim 7.0$ and $M_{\rm A} \sim 0.7$) with $\mathbf{B}_{\rm ext}$ perpendicular to the line of sight. The complete map (512×512 pixels) (*Upper-left*) and the zoomed regions (100×100 pixels). The sensitivity in simulated observations is assumed to be 0.3 of the maximum emission. Here, regions where the signal is less than 0.3 do not show polarization vectors, and $P_{\rm max} = 97\%$.

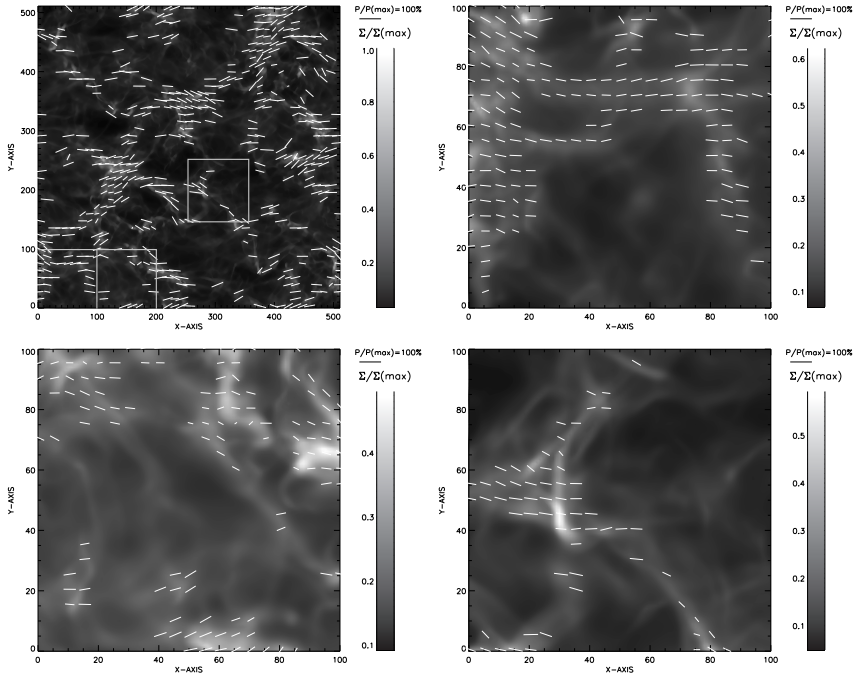

Fig. 2. Polarization of emission and column density maps for Model 4 ($M_{\rm S} \sim 7.0$ and $M_{\rm A} \sim 7.0$) with $\mathbf{B}_{\rm ext}$ perpendicular to the line of sight. The complete map (512×512 pixels) (*Upper-left*) and the zoomed regions (100×100 pixels). The sensitivity in simulated observations is assumed to be 0.3 of the maximum emission. Here, regions where the signal is less than 0.3 do not show polarization vectors, and $P_{\rm max} = 97\%$.

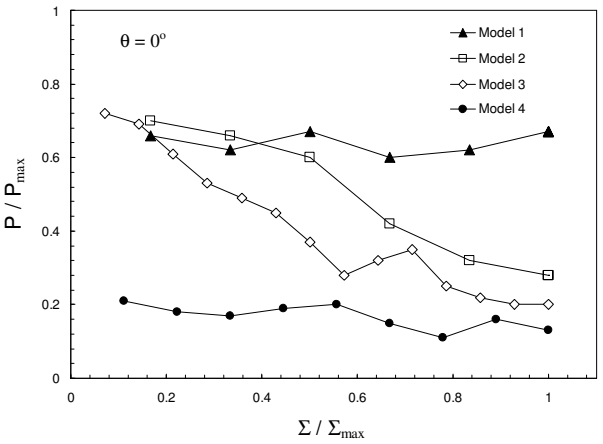

Fig. 3. Correlation between averaged polarization degree and the column density for the different models (FLK08). $P_{\rm max}$ is 100%, 98%, 97% and 85% for Model 1, 2, 3 and 4, respectively (FLK08).

In Figure 3 we show the correlation between the polarization degree and the column density for the different models, assuming that the magnetic field is in the plane of the sky. For all models, the polarization of high column densities tend to decrease to the minimum value ($\sim$ 20% $P_{\rm max}$). This minimum polarization degree should be zero for homogeneous density and random magnetic field. In inhomogeneous media it depends on the number of dense structures intercepted by the line of sight. The major contribution for the polarized emission comes from dense clumps, which only are few along the LOS. This poor statistics results in a non-zero polarization degree. We also noticed that in subsonic turbulence the polarization degree is large even for the higher column densities. It occurs because in the subsonic models the contrast in density is small and the simulated domain is more homogeneous. Also, the number of dense clumps, which are able to tangle the field lines, is reduced in the sub-sonic case. On the contrary, for the super-Alfvenic case we obtain the minimum polarization degree everywhere, i.e. purely random magnetic field components. For the decreasing part of the plots, we obtained a best fit with a correlation exponent $\gamma = 0.5$. If grain alignment was properly implemented in the calculations, the value of γ should increase.

3.2. *Statistics of Polarization Angles*

The histograms of polarization angles are shown in Figure 4. In the upper panel we show the histograms for the sub-Alfvenic (Models 1, 2 and 3) and the super-Alfvenic (Model 4) cases, with the mean magnetic field lines perpendicular to the LOS. The polarization angles present very similar distributions and almost equal dispersion for the sub-Alfvenic cases. This happens mainly because they do not depend on the density structures, but on the magnetic topology. Strongly magnetized turbulence creates more filamentary and smoother density structures (i.e. low density contrast) if compared to weakly magnetized models and, most importantly the magnetic field lines are not highly perturbed. For Model 4, the distribution is practically homogeneous, which means that the polarization is randomly oriented in the plane of sky. It occurs because the turbulent/kinetic pressure is dominant and the gas is able to easily distort the magnetic field lines.

In the bottom panel of Figure 4 we show the polarization angle histograms obtained for Model 3 but for different orientations of the magnetic field. The dispersion of the polarization angle is very similar for inclination angles $\theta < 60^\circ$, and increases for larger inclinations. It may be understood if it is noted that the projected magnetic field $B_{\rm sky} = B_{\rm ext}\cos\theta$ is of order of the random component δB. It shows that the dominant parameter that differ the distributions of ϕ is the uniform magnetic field projected in the plane of sky, and not the intensity of the global magnetic field.

Another statistical analysis, which helps us to understand the topology of the polarization angles, is based on structure functions. The second order structure function (SF) of the polarization angles is defined as the average of the squared difference between the polarization angle measured at 2 points separated by a distance l:

$$\mathrm{SF}(l) = \left\langle \left|\phi\left(\mathbf{r}+\mathbf{l}\right) - \phi\left(\mathbf{r}\right)\right|^2 \right\rangle . \qquad (5)$$

The structure functions calculated for the different models are shown in Figure 5. In the upper panel we present the SFs obtained for Model 3 with different values of θ. As expected, all curves present a positive slope showing the increase in the difference of polarization angle for distant points. However, the small scales part of the SF presents a plateau extending up to $l \sim 4-5$ pix. This range corresponds to the dissipation region and may also be related to the smallest turbulent cells. Surprisingly, the log-log slopes are equal independently on the inclination of the LOS (for l between 3 and 20 grid points). The same behavior was obtained for all models. In the bottom panel we show the SFs calculated for the different models with $\theta = 0$. It is noticeable the increase in the SF for higher Mach numbers. However, the slopes are notably different. The maximum slope is $\alpha \sim 1.1$, 0.8, 0.5 and 0.3 for Models 1, 2, 3 and

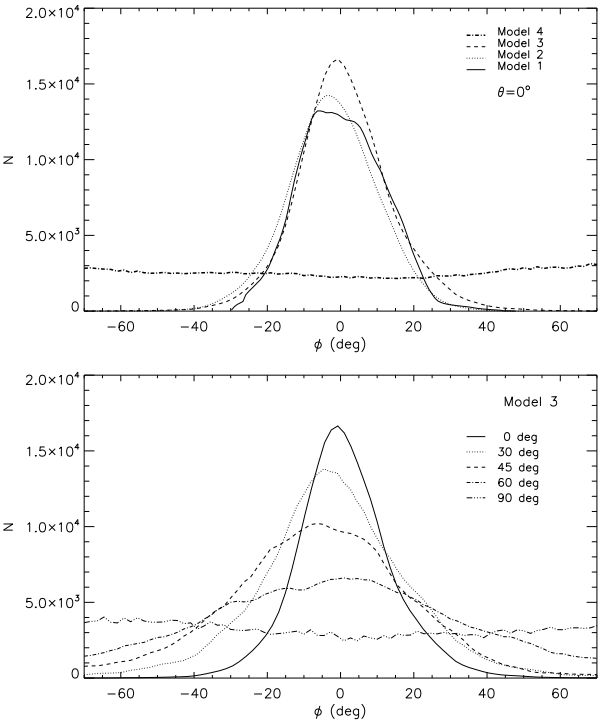

Fig. 4. Histograms of polarization angle of the different models with $\theta = 0$ (*up*), and for Model 3 and different magnetic field orientations in respect to the line of sight (angles θ) (*bottom*) (FLK08).

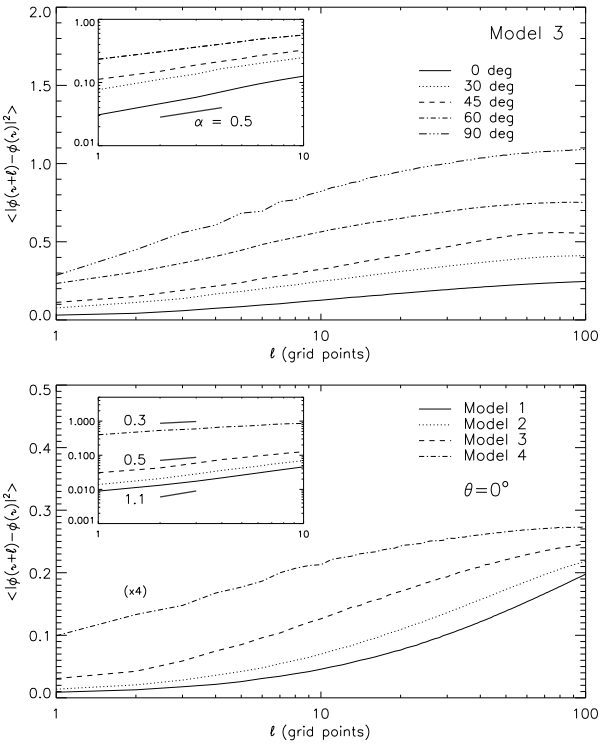

Fig. 5. Structure functions of polarization angle for Model 3 with different magnetic field orientations regarding the line of sight (angles θ) (*up*), and for the different models with magnetic field perpendicular to the line of sight ($\theta = 0$) (*bottom*)(FLK08).

4, respectively. Observationally, the molecular cloud M17 shows $\alpha \sim 0.5$ up to $l = 3$pc (Dotson 1996), which would be in agreement with a cloud excited by supersonic and sub(or critically)-Alfvenic turbulence.

3.3. *The Chandrasekhar-Fermi Method*

Chandrasekhar & Fermi (1953) proposed a method to estimate the ISM magnetic fields based on the dispersion of polarization angles and the rms velocity. Basically, it is assumed that the magnetic field perturbations are Alfvenic, i.e. $\delta v \propto \delta B\sqrt{\rho}$. If the rms is isotropic, we may relate both as:

$$B_u \sim \frac{1}{2}\sqrt{4\pi\rho}\,\frac{\delta V_{\rm LOS}}{\delta\phi}\,, \qquad (6)$$

If one wants to expand the applicability of the CF method for cases where the random component of the magnetic field is comparable to the uniform component, or for larger inclination angles, it is necessary to take into account two corrections. Firstly, we must introduce the total magnetic field projected in the plane of sky $B_{\rm sky} \sim B^{\rm ext}_{\rm sky} + \delta B$, where $B^{\rm ext}_{\rm sky}$ represents the mean field component projected on the plane of sky. We assume here, for the sake of simplicity, that δB is isotropic. We assume that the $\delta B/B$ is a global relation and, in this case, we may firstly obtain the dispersion of ϕ and then calculate its tangent. Substituting $\delta\phi$ in equation (6) by $\tan(\delta\phi) \sim \delta B/B_{\rm sky}$, we obtain the modified CF equation:

$$B^{\rm ext}_{\rm sky} + \delta B \simeq \sqrt{4\pi\rho}\,\frac{\delta V_{\rm los}}{\tan\left(\delta\phi\right)}\,. \qquad (7)$$

Since the CF-method strongly depends on the resolution (bacause of the dispersion of angles and velocities), we applied equation (7) to our simulated clouds, taking into account the effects of finite resolution. We calculated the average of the density weighted rms velocity along the LOS ($\delta V_{\rm los}$) and the dispersion of the polarization angle ($\delta\phi$) within regions of $R \times R$ pixels. To simulate a real cloud we substitute the parametric values of the Model 3 for $n_{\rm H} = 10^3{\rm cm}^{-3}$ and $T = 10$K, and $B \sim 50\mu$G. The results showed a correlation between the obtained magnetic field from equation (7) and the resolution,

TABLE 2

CF METHOD ESTIMATES

Model	$\theta(^\circ)$	C	$B^0_{\rm CF}/B_{\rm ext}$	$B^{\rm ext}_{\rm sky}/B_{\rm ext}$	$B_{\rm tot}/B_{\rm ext}$
3	0	20 ± 5	1.24 ± 0.09	1.00	1.25
3	30	24 ± 5	0.98 ± 0.08	0.87	1.11
3	45	25 ± 5	0.78 ± 0.07	0.71	0.96
3	60	33 ± 5	0.48 ± 0.05	0.50	0.75
3	90	31 ± 5	0.26 ± 0.03	0.00	0.24
1	0	7 ± 5	0.97 ± 0.08	1.00	1.11
2	0	10 ± 5	1.07 ± 0.07	1.00	1.16
4	0	34 ± 5	1.18 ± 0.07	1.00	1.41

which may be described by:

$$B_{\rm CF} = B^0_{\rm CF}\left(1 + \frac{C}{R^{0.5}}\right), \qquad (8)$$

where R represents the observational resolution (total number of pixels), C and $B^0_{\rm CF}$ are constants obtained from the best fit. $B^0_{\rm CF}$ represents the value of $B_{\rm CF}$ for infinite resolution observations, i.e. the best magnetic field estimation from the CF method.

The fit parameters, as well as the expected values of the magnetic field from the simulations for all models, are shown in Table 2. Here, the magnetic fields are given in units of the mean field $B_{\rm ext}$. Since the simulations are scale independent, one could choose values of $B_{\rm ext}$ to represent a real cloud, in accordance with the parameters of Table 1. As an example, assuming a cloud with $n_{\rm H} = 10^3{\rm cm}^{-3}$ and $T = 10$K, and $\beta = 0.01$ (Model 3), we get $B \sim 50\mu$G. Choosing differently the density, temperature or the model given by the simulations, i.e. β, we obtain a different mean magnetic field. The obtained parameter C is very similar for the different inclinations, but are different depending on the model, mainly because it is related to the scale on which the dispersion of the polarization angle changes. Since C seems to depend on the model and not on the inclination it could also be used by observers to infer the physical properties of clouds from polarization maps.

As a practical use, observers could obtain polarimetric maps of a given region of the sky for different observational resolutions (e.g. changing the resolution via spatial averaging). Using the CF technique for each resolution and, then apply equation (8) to determine the asymptotic value of the magnetic field projected into the plane of sky $B^0_{\rm CF}$.

4. CONCLUSIONS

In this work we presented turbulent 3-D high resolution MHD numerical simulations in order to study the polarized emission of dust particles in molecular clouds. We obtained synthetic dust emission polarization maps calculating the Stokes parameters Q, U and I assuming a perfect grain alignment and that the dust optical properties are the same at all cells. Under these conditions, we were able to study the polarization angle distributions and the polarization degree for the different models and for different inclinations of the magnetic field regarding the LOS.

As main results, we obtained an anti-correlation between the polarization degree and the column density, which is in agreement with observations, with exponent $\gamma \sim -0.5$. This value is related to random cancellation of polarization vectors integrated along the LOS, while larger indices require extra physics, e.g. dependency of the dust alignment efficiency with the local density.

We showed that the overall properties of the polarization maps are related to the Alfvenic Mach number and not to the magnetic to gas pressure ratio. Also, we studied the PDF's and structure functions of the polarization angles, which showed a degeneracy of the results with the Alfvenic Mach number and the angle between the magnetic field and the LOS. Zeeman measurements of dense clouds may be useful to help remove this degeneracy as it could provide the magnetic field component along the LOS and, therefore, the inclination.

Finally, we presented a generalization of the CF method, which was showed to be useful for: (i) the determination of the total magnetic field projected in the plane of sky, and (ii) the separation of the two components $B_{\rm sky}$ and δB.

D.F.G., A.L. and G.K. thank the financial support of the NSF (No. AST0307869), the Center for Magnetic Self-Organization in Astrophysical and Laboratory Plasmas and the Brazilian agencies FAPESP (No. 06/57824-1 and 07/50065-0) and CAPES (No. 4141067).

REFERENCES

Chandrasekhar, S. & Fermi, E. 1953, ApJ, 118, 113
Crutcher, R. M., Roberts, D. A., Troland, T. H. & Goss, W. M. 1999, ApJ, 515, 275
Dotson, J. 1996, ApJ, 470, 566
Falceta-Gonçalves, D., Lazarian, A. & Kowal, G. 2008, ApJ, 679, 537 (FLK08)
Girart, J. M., Rao, R. & Marrone, D. P. 2006, Science, 313, 812
Gonçalves, J., Galli, D. & Walmsley, M. 2005, A&A, 430, 979
Hildebrand, R. H., Davidson, J. A., Dotson, J. L., Dowell, C. D., Novak, G., & Vaillancourt, J. E. 2000, PASP, 112, 1215
Kowal, G., Lazarian, A. & Beresniak, A. 2007, ApJ, 658, 423
Lai, S.-P., Girart, J. M. & Crutcher, R. M. 2003, ApJ, 598, 392
Matthews, B. C. & Wilson, C. D. 2002, ApJ, 574, 822
Ostriker, E. C., Stone, J. M. & Gammie, C. F. 2001, ApJ, 546, 980
Padoan, P., Goodman, A., Draine, B. T., Juvela, M., Nordlund, A. & Rognvaldsson, Ö. E. 2001, ApJ, 559, 1005
Padoan, P. & Norlund, A. 2002, ApJ, 576, 870
Pelkonen, V.-M., Juvela, M. & Padoan, P. 2007, ApJ, 461, 551
Schleuning, D. A. 1998, ApJ, 493, 811
Wolf, S., Launhardt, R. & Henning, T. 2003, ApJ, 592, 233